# Electrochemical Studies of Structurally Related Triply-Bridged Dinuclear Tris(bipyridine)iron(II) Complexes: An Electrostatic Model for Site−Site Interaction

**Suzanne Ferrere[†] and C. Michael Elliott***

Department of Chemistry, Colorado State University, Fort Collins, Colorado 80523

*Received May 19, 1995*[⊗]

The structures and electrochemical behavior of a series of symmetric dinuclear complexes in which two iron centers are bridged by *three* bis[4-(4′-methyl-2,2′-bipyridinyl)]alkane ligands are presented. Square wave voltammetry was used to characterize the extent of interaction between the metal-centered halves. Because the saturated linkages preclude significant electron delocalization, the observed interaction is concluded to be almost purely Coulombic in nature. Furthermore, molecular modeling and X-ray crystallographic data confirm that the iron−iron separation in the complex containing three methylenes in the linkages is nearly identical to the iron−iron separation in the complex containing two methylenes in the linkages. Using a simple electrostatic model and employing structural parameters obtained from X-ray data and molecular modeling, the electrochemical trends within the series are interpreted.

## Introduction

Numerous examples of symmetric dinuclear transition metal complexes can be found in the literature.[1,2] When these complexes undergo chemically reversible redox reactions it is generally possible to prepare and study their mixed-valence forms. The spectral and electrochemical behavior of such dinuclear species is determined by the mechanism and extent of the interactions between metal-centered halves.[3] Electrochemical techniques have, in the past, been used to characterize symmetric dinuclear metal complexes. The voltammetric behavior of such complexes is determined partly by the degree of electron delocalization. Taube and Sutton have pointed out, however, that the degree of comproportionation which exists in a formally mixed-valent dinuclear complex (and, thus the voltammetric wave shapes) is also influenced by electrostatic interactions.[2] In other words, when the complex is charged, each half of the molecule exerts a Coulombic influence on the other half irrespective of any electron delocalization. While the existence of these electrostatic interactions has long been recognized, it has typically been difficult to quantitate the effect because, generally, it is not possible to separate the purely Coulombic part of the interaction from effects due to electron delocalization. Historically, in systems that could be demonstrated to be nearly rigorously valence-localized (i.e., Robin and Day, Class I)[3] the metal centers are typically separated by large distances; consequently, Coulombic interactions are also vanishingly small.

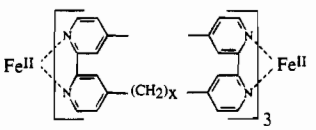


"[Fe$_2$(4X0)$_3$]$^{4+}$"

I. X = 2
II. X = 3
III. X = 4

**Figure 1.** Diiron complexes containing bridging alkyl chains and abbreviated nomenclature employed.

In an earlier study we reported the X-ray structure and electrochemical behavior of a symmetric dinuclear iron complex consisting of two tris(bipyridine)iron(II) moieties bridged by three saturated two-carbon alkyl linkages (Figure 1, **I**).[4] Because of the triply-bridged nature of this complex, the metal centers are held considerably closer together (an Fe−Fe separation of 7.646(3) Å) than in singly linked analogs. We concluded in this earlier study that the interactions observed in this complex

* To whom correspondence should be addressed.

[†] Current address: National Renewable Energy Laboratory, Golden, CO 80401.

[⊗] Abstract published in *Advance ACS Abstracts,* November 1, 1995.

(1) Literally thousands of references to bridged homo- and heterodinuclear metal complexes have appeared within the last few years. Some selected examples more relevant to the present study are as follows: (a) Fischer, H.; Tom, G. M.; Taube, H. *J. Am. Chem. Soc.* **1976**, *98*, 5512. (b) Rieder, K.; Taube, H. *J. Am. Chem. Soc.* **1977**, *99*, 7891. (c) Callahan, R. W.; Keene, F. R.; Meyer, T. J.; Salmon, D. J. *J. Am. Chem. Soc.* **1977**, *99*, 1064. (d) Tanner, M.; Ludi, A. *J. Am. Chem. Soc.* **1981**, *20*, 2350. (e) Tinnemans, A. H. A.; Timmer, K.; Reinten, M.; Kraaijkamp, J. G.; Alberts, A. H.; van der Linden, J. G. M.; Schmitz, J. E. J.; Saaman, A. A. *Inorg. Chem.* **1981**, *20*, 3698. (f) Richardson, D. E.; Taube, H. *J. Am. Chem. Soc.* **1983**, *105*, 40. (g) Geno, M. J. K.; Dawson, J. H. *Inorg. Chem.* **1984**, *23*, 1182. (h) Yao, Y.; Perkovic, M. W.; Rillema, D. P.; Woods, C. *Inorg. Chem.* **1992**, *31*, 3956. (i) Haga, M.; Bond, A. M. *Inorg. Chem.* **1991**, *30*, 475. (j) De Cola, L.; Belser, P.; Ebmeyer, F.; Barigelletti, F.; Voegtle, F.; Von Zelewsky, A; Balzani, V. *Inorg. Chem.* **1990**, *29*, 495. (k) Hupp, J. T.; Neyhart, G. A.; Meyer, T. J.; Kober, E. M. *J. Phys. Chem.* **1992**, *96*, 10820. (l) Dong, Y.; Hupp, J. T. *Inorg. Chem.* **1992**, *31*, 3322. (m) Hupp, J. T.; Dong, Y.; Blackbourn, R. L.; Lu, H. *J. Phys. Chem.* **1993**, *97*, 3278. (n) Van Wallendael, S.; Shaver, R. J.; Rillema, D. P.; Yoblinski, B. J.; Stathis, M.; Guarr, T. F. *Inorg. Chem.* **1990**, *29*, 1761. (o) Shaw, J. R.; Webb, R. T.; Schmehl, R. H. *J. Am. Chem. Soc.* **1990**, *112*, 1117. (p) Kaim, W.; Bruns, W.; Kohlmann, S.; Krejcik, M. *Inorg. Chim. Acta* **1995**, *229*, 143. (q) Kasack, V.; Kaim, W.; Binder, H.; Jordanov, J.; Roth, E. *Inorg. Chem.* **1995**, *34*, 1924. (r) Haga, M.; Ali, M. M.; Koseki, S.; Yoshimura, A.; Nozaki, K.; Ohno, T. *Inorg. Chim. Acta* **1994**, *226*, 17. (s) Haga, M.; Ali, M. M.; Maegawa, H.; Nozaki, K.; Yoshimura, A.; Ohno, T. *Coord. Chem. Rev.* **1994**, *132*, 89. (t) De Cola, L.; Barigelletti, F.; Balzani, V.; Belser, P.; Von Zelewsky, A.; Frank, M.; Voegtle, F. *Mol. Cryst. Liq. Cryst. Sci. Technol. Sect. A* **1993**, *234*, 115. (u) De Cola, L.; Balzani, V.; Barigelletti, F.; Flamigni, L.; Belser, P.; von Zelewsky, A.; Frank, M.; Voegtle, F. *Inorg. Chem.* **1993**, *32*, 5228. (v) Molnar, S. M.; Neville, K. R.; Jensen, G. E.; Brewer, K. J. *Inorg. Chim. Acta* **1993**, *206*, 69. (w) Richter, M. M.; Brewer, K. J. *Inorg. Chem.* **1993**, *32*, 2827. (x) Haga, M.; Ano, T.; Kano, K.; Yamabe, S. *Inorg. Chem.* **1991**, *30*, 3843.

(2) (a) Sutton, J. E.; Sutton, P. M.; Taube, H. *Inorg. Chem.* **1979**, *18*, 1017. (b) Sutton, J. E.; Taube, H. *Inorg. Chem.* **1981**, *20*, 3125−3134.

(3) Robin, M. B.; Day, P. *Adv. Inorg. Chem. Radiochem.* **1967**, *10*, 247.

(4) Serr, B. R.; Andersen, K. A.; Elliott, C. M.; Anderson, O. P. *Inorg. Chem.* **1988**, *27*, 4499.

0020-1669/95/1334-5818$09.00/0 

and manifested by its electrochemical behavior were virtually purely Coulombic in nature. We have since prepared two additional complexes which differ from the previously reported diiron complex, **I**, in the number of atoms in the three alkyl bridges (Figure 1, **II** and **III**). Preliminary X-ray structural studies and molecular modeling calculations indicate that the Fe(II)/Fe(II) form of **I** and **II** have very similar metal−metal separations despite the differences in the linkages. In contrast, the metal−metal separation in **III** is considerably greater. Below we compare the electrochemical results for these three complexes and consider their behavior in terms of a simple electrostatic interaction model.

## Experimental Section

**Measurements.** Standard electrochemical measurements were carried out in $O_2$-free, nitrogen-purged acetonitrile solutions with 0.1 M tetra-*n*-butylammonium hexafluorophosphate [(TBA)$PF_6$] as supporting electrolyte. Cyclic voltammetry and Osteryoung square wave voltammetry were performed with a BAS-100 Electrochemical Analyzer employing a conventional three-electrode cell with a 7.1 $mm^2$ glassy-carbon disk working electrode, a platinum wire loop auxiliary electrode, and a saturated calomel electrode (SCE) as reference.

Microelectrode voltammetry was performed at a 10 $\mu$m gold disk working electrode with a silver wire reference electrode; no auxiliary electrode was employed. The concentration of supporting electrolyte [(TBA)$PF_6$] was varied. The fast scan potentiostat was controlled with an EG&G PAR Model 175 universal progammer.[5] Both the potentiostat and the electrochemical cell were housed in a Faraday cage. The output was digitized on a Nicolet 3091 digital oscilloscope, then recorded on a Houston Instruments Omnigraphic 2000 recorder.

Molecular modeling was carried out at a Silicon Graphics workstation, employing Biograf software (MSI). The Dreiding force field was employed.[6a] Partial charges were obtained using QEq.[6b] Annealed dynamics was used as the conformational searching procedure.[6c]

Elemental analyses were performed by Desert Analytics, Tucson, AZ.

**Materials.** All reagents and solvents were purchased commercially and used without further purification except for the following: [(TBA)$PF_6$] was prepared according to a previously published procedure,[7] recrystallized three times from hot ethanol, and dried under vacuum. 4,4′-Dimethyl-2,2′-bipyridine (DMB), obtained from Reilley Tar and Chemical, Indianapolis, IN, was recrystallized from ethyl acetate before use. Butyllithium (Aldrich) was standardized before use. Tetrahydrofuran was distilled under $N_2$ from $Na^0$/benzophenone. Dibromomethane was distilled before use.

1,2-Bis[4-(4′-methyl-2,2′-bipyridinyl)]ethane (**420**)[8] and [Fe(DMB)$_3$][$PF_6$]$_2$ were prepared as previously described.[4,9]

**Preparation of 1,3-Bis[4-(4′-methyl-2,2′-bipyridinyl)]propane (430).**[8] In a typical preparation, ~30 mL of dry, distilled THF was transferred via cannula under $N_2$ into a 3-neck 1 L round-bottomed flask, and the flask was immersed in a dry ice/acetone bath (−78 °C). To this, 7.62 mL of diisopropylamine (0.054 mol, dried by passing through an alumina column) and 23 mL of 2.4 M *n*-butyllithium (0.054 mol) were added and the mixture stirred under $N_2$ for ~15 min. Then, 10 g (0.054 mol) of 4,4′-dimethyl-2,2′-bipyridine, dissolved in 500 mL of dry, distilled THF, were added dropwise over a period of ~15 min. This dark purple mixture was allowed to stir for approximately 2 h under $N_2$, while the dry ice bath was maintained. Dibromomethane (1.90 mL, 0.027 mol) was added via syringe. The dry ice bath was removed, and the mixture was allowed to warm to room temperature. Finally, the reaction was quenched by the addition of a small amount of either methanol or water. Several hundred milliliters of water were added to the reaction mixture, which was then extracted several times with ether and then dichloromethane. The organic fractions were extracted with water, brought to dryness by rotary evaporation, and vacuum dried overnight. Column chromatography in 10−30% acetone/dichloromethane on silica gel yielded a light brown oil, which was recrystallized from absolute ethanol to yield white crystals. Typical yield: 2 g (20%) $^1$H NMR ($\delta$, ppm from TMS, $CDCl_3$): 2.0 (quintet, 1H); 2.3 (s, 3H); 2.65 (t, 2H); 7.0 (d of d, 2H); 8.1 (s, 2H); 8.45 (d of d, 2H).

**Preparation of 1,4-Bis[4-(4′-methyl-2,2′-bipyridinyl)]butane (440).**[8] Preparation of this ligand was identical to the preparation of the **430** ligand above, except that a solution of ethylene glycol di-*p*-tosylate (10.0 g dissolved in ~300 mL THF) was added via cannula to the carbanion mixture in place of dibromomethane. Workup was also the same as that for the **430** ligand. Column chromatography in 10−30% acetone/dichloromethane on silica gel followed by recrystallization of the crude product from ethyl acetate yielded white crystals. Typical yield: 3 g (30%) $^1$H NMR ($\delta$, ppm from TMS, $CDCl_3$): 1.76 (quintet, 2 H); 2.42 (s, 3H); 2.72 (t, 2H); 7.13 (t, 2H); 8.23 (s, 2H); 8.56 (t, 2H).

**Preparation of [$Fe^{II}$(420)$_3$$Fe^{II}$][$PF_6$]$_4$ (I).** The complex was prepared as previously reported.[4] Anal. Calcd for $Fe_2C_{72}N_{12}H_{66}P_4F_{24}$: C, 48.29; H, 3.71; N, 9.38. Found: C, 48.56; H, 4.10; N, 9.41.

**Preparation of [$Fe^{II}$(430)$_3$$Fe^{II}$][$PF_6$]$_4$ (II).** In a typical preparation, 150 mg (3 equiv) of the **430** ligand were dissolved in acetone and heated in an Erlenmeyer flask while degassing with nitrogen. A 263 mL aliquot of aqueous $1 \times 10^{-3}$ M $FeSO_4$ solution (2 equiv) was pipetted into the acetone solution. The solution immediately, upon addition of the $Fe^{2+}$, turned dark blood red with some solid, presumably polymeric, material present. The solution was brought to reflux, allowing the acetone to boil off. The reaction was refluxed under $N_2$ flow for approximately 1 h during which time all of the insoluble material went into solution. Completion of reaction was verified by silica TLC employing 5:4:1 $CH_3CN$:$H_2O$:$KNO_3$(saturated aqueous) as the eluent, in which the desired dinuclear product has an $R_f \sim 0.75$. The aqueous solution was then allowed to cool to room temperature and the product precipitated as the $PF_6^-$ salt by the addition of saturated $NH_4PF_6$. The product mixture was collected on a medium frit or in a centrifuge tube as a dark red solid, then vacuum dried overnight. Silica gel column chromatography in 5:4:1 $CH_3CN$:$H_2O$:$KNO_3$ (saturated aqueous) was performed to obtain purified product. Purity was verified by TLC and electrochemistry (cyclic and square wave voltammetry). Yields were usually ~75%. Anal. Calcd for $Fe_2C_{75}N_{12}H_{72}P_4F_{24}$: C, 49.14; H, 3.96; N, 9.17; Fe, 6.09; F, 24.87. Found: C, 49.06; H, 4.03; N, 9.17; Fe, 5.80; F, 24.67.

**Preparation of [$Fe^{II}$(440)$_3$$Fe^{II}$][$PF_6$]$_4$ (III).** Preparation of this complex was identical to complex **II**, except that typically, 150 mg (3 equiv) of 440 ligand and 253 mL of an aqueous $1 \times 10^{-3}$ M $FeSO_4$ solution (2 equiv) were utilized in the reaction. Yields were usually ~80%. Anal. Calcd for $Fe_2C_{78}N_{12}H_{78}P_4F_{24}$: C, 49.96; H, 4.19; N, 8.96. Found: C, 49.37; H, 4.31; N, 8.46.[10]

**Preparation of [Ru(DMB)$_3$][$PF_6$]$_2$.** Typically, 200 mg of 4,4′-dimethyl-2,2′-bipyridine was dissolved in ~50 mL degassed absolute ethanol and brought to refluxing temperature. To this solution, 159 mg of $Ru(DMSO)_4Cl_2$ was added and the mixture refluxed for 2 h. The ethanol was then rotary evaporated and the bright orange reaction

(5) (a) Dayton, M. A.; Brown, J. C.; Stutts, K. J.; Wightman, R. M. *Anal. Chem.* **1980**, *52*, 946. (b) Howell, J. O.; Wightman, R. M. *Anal. Chem.* **1984**, *56*, 524.

(6) (a) Mayo, S. L.; Olafson, B. D.; Goddard, W. A. *J. Phys. Chem.* **1990**, *94*, 8897. (b) Rappé, A. K.; Goddard, W. A.; *J. Phys. Chem.* **1991**, *95*, 3358. (c) Castonguay, L. A.; Rappé, A. K. *J. Am. Chem. Soc.* **1992**, *114*, 5832.

(7) Elliott, C. M.; Hershenhart, E.; Finke, R. G.; Smith, B. L. *J. Am. Chem. Soc.* **1981**, *103*, 5558.

(8) The numerical abbreviations used to designate the three bisbipyridylalkane ligands, **420**, **430**, and **440**, are derived from designation of related ligands published earlier. The first digit indicates the position of the linkage on the pyridine ring (i.e., the 4-position), the second digit is the number of methylenes in the alkyl chain, and the third digit (i.e., "0") simply indicates that none of the pyridine nitrogens are quaternarized—a holdover from previous work.

(9) Elliott, C. M.; Freitag, R. A.; Blaney, D. D. *J. Am. Chem. Soc.* **1985**, *107*, 4647−4655.

(10) The reported analytical data for complex **III** is slightly outside of acceptable limits. Of all of the dinuclear complexes **III** is the least crystalline and, consequently, the most difficult to wash and dry completely prior to analysis. However, based on all other criteria (e.g., electrochemistry, NMR, TLC) we are confident that **III** is correct as formulated and the slight deviation in the elemental analysis is due to small amounts of either salt or water which are entrained in the solid.

mixture redissolved in ~50 mL of distilled water. This solution was filtered to recover insoluble unreacted ligand. The product was precipitated from the filtrate by addition of several drops of saturated $NH_4PF_6$. The orange product was collected on a medium frit, rinsed several times with ~20 mL portions of distilled water, and then rinsed several times with ~20 mL portions of toluene. The pure product was vacuum dried overnight. Purity was verified by TLC and electrochemistry.

**Preparation of $[Ru(420)_3][PF_6]_2$.** Typically, 366 mg of **420** ligand was dissolved in ~75 mL degassed absolute ethanol and brought to refluxing temperature. To this solution, 19.38 mg ($^1/_{25}$th of an equivalent) of $Ru(DMSO)_4Cl_2$ was added and the mixture refluxed for 2 h. The ethanol was then rotary evaporated and the bright orange reaction mixture redissolved in ~75 mL distilled water. This solution was filtered to recover insoluble unreacted ligand. The product was precipitated from the filtrate by the addition of several drops of saturated $NH_4PF_6$. The orange product was collected on a medium frit, rinsed several times with ~20 mL portions of distilled water, then several times with ~20 mL portions of toluene. The pure product, obtained as a mixture of *fac* and *mer* isomers, was vacuum-dried overnight. Purity was verified by TLC, electrochemistry, and ES-MS.

**Preparation of $[Ru(430)_3][PF_6]_2$.** Preparation and characterization of this complex was identical to the preparation of $[Ru(420)_3][PF_6]_2$ except that, typically, 380 mg of **430** ligand was employed in the reaction.

## Methods

**Molecular Modeling.** Molecular dynamics were run for each diiron complex. The structures were either constructed "by hand" using Biograf or the X-ray crystal structure of **I** was imported from the Cambridge database into the program and modified in the cases of complexes **II** and **III**. The complexes were modeled as both crystals (i.e., fixed counterion distances) and solution species. For dynamics runs, the type of dynamics and/or the counterion environment around the iron species was varied. The parameters for the resulting minimized structures, regardless of the method or how the structures were originally entered, were similar. In particular, the trends within the series were always the same. As an indication of the validity of modeling, the iron−iron distance for all minimized forms of the low energy structures of the **420** complex was found to be within ±0.10 Å of the distance obtained from the X-ray crystal structure.

**Crystallographic Study.** Crystals of **II** were prepared by vapor diffusion of pentane into a solution of acetone containing ~$10^{-3}$ M of $[Fe(430)_3][SO_3CF_3]_4$. A Siemens P4 diffractometer equipped with an LT-2 variable temperature accessory was used to collect data (crystals: clear dark red needles). The 0.41 mm × 0.20 mm × 0.10 mm crystal was embedded in vacuum grease and mounted on a glass fiber in the −100 °C nitrogen stream. The centering of 25 reflections gave the trigonal unit cell dimensions $a$ = 17.323(3) Å and $c$ = 21.298(3) Å and a cell volume of 5535.2(16) Å$^3$. The space group chosen was $P\bar{3}1c$. Using Siemens SHELXTL/Unix and an isotropic model that included only the structure of the cation refinement proceeded to an $R$ value of 21%. Details of the structure are not reported because the anions were severely disordered. Attempts to model the disordered anions were completely unsuccessful. However, the cationic portion of the molecule was successfully modeled, even down to the level of a 50/50 disorder in the central methylene carbon atom of the connecting bridge.

## Results

**X-ray Crystallography.** Despite numerous attempts employing a wide range of solvents and counterions, efforts to obtain diffraction quality crystals of **II** were only marginally successful. The disorder in the four triflate anions was so severe that it was impossible to determine even their nominal positions (which is probably largely responsible for the poor $R$ factor). The straightforward solution to give a chemically reasonable structure for the cation is convincing evidence that this portion of the structure can be relied on provided one does not insist on too great a level of metric detail. The iron−iron distance obtained from consideration of this structure is 7.6 Å, in agreement with the distance obtained from molecular modeling calculations (below). Furthermore, the position and orientation of the bipyridine ligands also closely matches their position in the modeled structure.

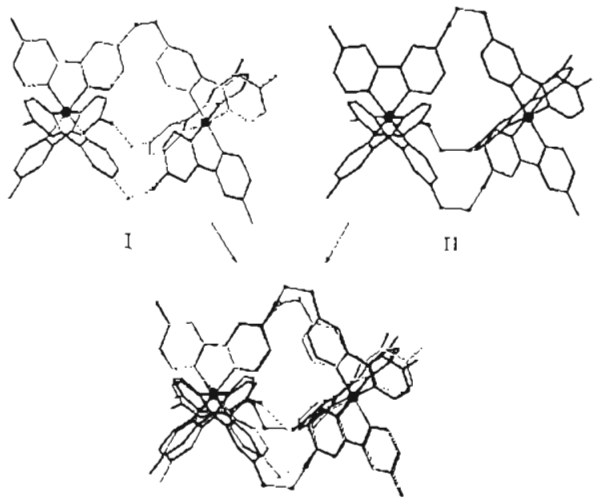


**Figure 2.** Structures of **I** and **II** obtained from molecular modeling calculations and their superpositions.

**Table 1.** Iron−Iron Distances Obtained from Molecular Modeling for $[Fe_2(4X0)_3^{4+}][SO_3CF_3]_4$ Complexes[a]

| complex | Fe−Fe (Å) |
|---|---|
| **420** | 7.59 ± 0.03 |
| **430** | 7.55 ± 0.07 |
| **440** | 9.08 ± 0.40 |

[a] 20 cycles annealed dynamics, 0−600 K. Minimized lowest energy structures.

**Molecular Modeling.** Annealed dynamics were run for 20 cycles utilizing a temperature ramp of 0−600 K. The structures obtained from each run were minimized. The iron−iron distances for the lowest energy structures obtained were averaged, and are presented in Table 1. These were modeled with four triflate counterions, which closely reproduces the crystal structure obtained for **I**, so that the structure (including the diiron complex and four surrounding triflates) had an overall charge of zero. The triflate counterions were constrained, to positions which mimic their positions in the crystal structure of **I**, to prevent them from "boiling away" in the dynamics run.

The modeled iron−iron distance obtained for **II**, despite the fact that the bridge has more carbons, is consistently somewhat smaller than the corresponding distance in the two-carbon bridged complex, **I** (Consistent with X-ray structural results above). This result is obtained regardless of the type of dynamics used.

Figure 2 shows the structures of **I** and **II** obtained from these calculations along with their superposition. When these modeled structures are compared with the corresponding X-ray structures, there is excellent agreement. These two structures for **I** are virtually identical. The modeled structure of **II** closely matches those positions of the X-ray structure that are not disordered (i.e., the metal centers and their coordinated bipyridines).

**Cyclic Voltammetry.** All of the iron complexes display four apparent redox processes: a metal-based, $Fe^{III/II}$ process located positive of 0.00 V and three ligand-based reductions negative of 0.00 V (Figure 3). The corresponding processes are reversible for the mononuclear analog, $[Fe(DMB)_3]^{2+}$. However, for all of the dinuclear complexes, each wave is considerably broader than for the mononuclear system. This is most apparent for **I** and **II**, as can be seen in Figure 3.

**Table 2.** Osteryoung Square Wave Voltammetry[a]

a. Individual $E_{1/2}$ Values from EE Analysis

| complex | $FeCp_2$ | oxidation | | reduction 1 | | reduction 2 | | reduction 3 | |
|---|---|---|---|---|---|---|---|---|---|
| | | $E_{1/2}(1)$ | $E_{1/2}(2)$ | $E_{1/2}(1)$ | $E_{1/2}(2)$ | $E_{1/2}(1)$ | $E_{1/2}(2)$ | $E_{1/2}(1)$ | $E_{1/2}(2)$ |
| $Fe(DMB)_3^{2+}$ | 0.380 | 0.904 | | −1.468 | | −1.656 | | −1.912 | |
| $Fe_2(\mathbf{420})_3^{4+}$ | 0.384 | 0.991 | 1.062 | −1.355 | −1.432 | −1.599 | −1.684 | −1.909 | −1.993 |
| $Fe_2(\mathbf{430})_3^{4+}$ | 0.384 | 0.956 | 1.029 | −1.367 | −1.446 | −1.603 | −1.691 | −1.923 | −2.004 |
| $Fe_2(\mathbf{440})_3^{4+}$ | 0.380 | 0.923 | 0.975 | −1.389 | −1.452 | −1.606 | −1.670 | −1.907 | −1.980 |

b. $\Delta E_{1/2}$ Values Obtained from OSWV Analysis

| complex | oxidation | reduction 1 | reduction 2 | reduction 3 |
|---|---|---|---|---|
| $Fe_2(\mathbf{420})_3^{4+}$ | 0.071 | 0.077 | 0.085 | 0.084 |
| $Fe_2(\mathbf{430})_3^{4+}$ | 0.073 | 0.079 | 0.088 | 0.081 |
| $Fe_2(\mathbf{440})_3^{4+}$ | 0.052 | 0.062 | 0.064 | 0.073 |

[a] Peak potentials in volts vs SCE. "Middle" values reported from triplicate analysis.

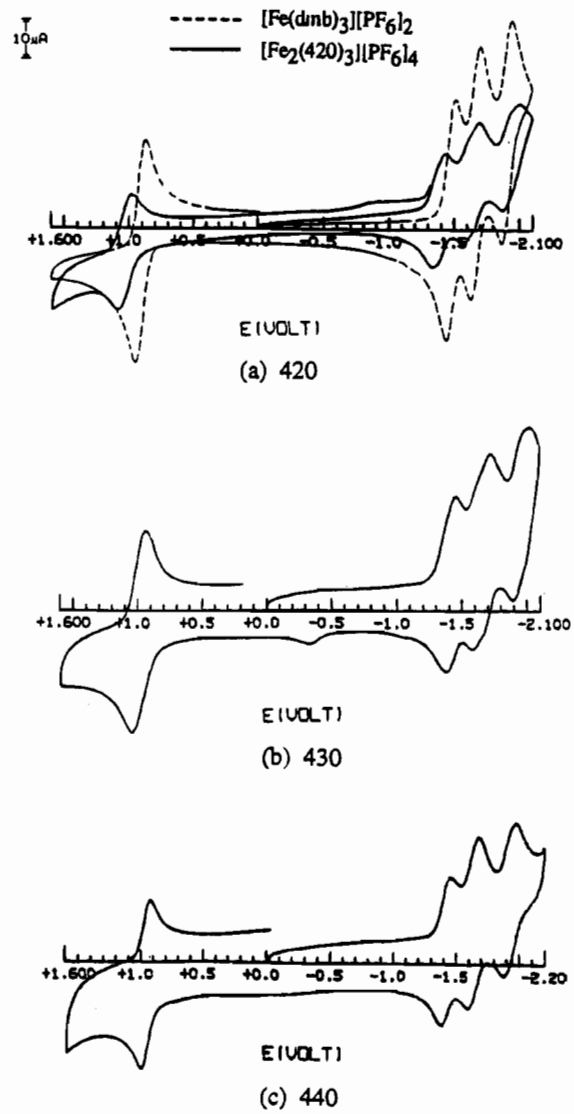


**Figure 3.** Cyclic voltammetry of $[Fe_2(\mathbf{4X0})_3][PF_6]_4$ complexes and $[Fe(DMB)_3][PF_6]_2$ (100 mV/s, acetonitrile/0.10 M $(TBA)PF_6$).

For the dinuclear complexes, each of these four broad waves is, in fact, a pair of closely-spaced, overlapping one electron waves slightly shifted in potential from one another. For example, the metal based oxidation consists of a 4+/5+ ($Fe^{II}$-$Fe^{II}/Fe^{II}Fe^{III}$) and a 5+/6+ ($Fe^{II}Fe^{III}/Fe^{III}Fe^{III}$) process which are separated slightly in potential from one another, by an amount, $\Delta E_{1/2}$ (*vide infra*).

**Osteryoung Square Wave Voltammetry.** As stated above, the individual processes are poorly resolved by cyclic voltammetry. In order to better resolve the individual processes, Osteryoung square wave voltammetry (OSWV) was employed. Not only does this technique partially resolve the individual waves visibly, but theoretical treatments of the data can yield the individual $E_{1/2}$ values for each redox process.

The OSWV data for each complex was analyzed employing an algorithm developed in the laboratory of Professor Janet G. Osteryoung at SUNY-Buffalo and at North Carolina State University (to whom we are greatly indebted for her kind assistance). This algorithm employs all of the experimental current data in the fit and gives the predicted response for a theoretically derived EE mechanism.[11] The values of $\Delta E_{1/2}$ and individual $E_{1/2}$ values obtained from this analysis are presented in Table 2.

Considering, for example, the metal-based oxidation processes, for each of the dinuclear complexes, both of the two oxidation processes (3+,3+/3+,2+ and 3+,2+/2+,2+) are, in general, more difficult than for the 3+/2+ couple of the mononuclear analog (i.e., they occur at more positive potentials). As stated above, the largest relative shifts occur for **I** (158 mV for the 3+,3+/3+,2+ process and 87 mV for the 3+,2+/2+,2+ process, respectively). With increasing numbers of methylenes in the alkane bridge the potential shift of each respective process relative to the mononuclear complex decreases *(vide infra)*.

**Microelectrode Voltammetry.** Fast scan ($v$ = 500 V/s) cyclic voltammetry was performed at a 10 $\mu$m gold electrode for the $[Fe_2(\mathbf{420})_3][PF_6]_4$ complex. The half-wave potential of the iron-based wave for varying concentrations of supporting electrolyte was recorded as the midway point between the anodic and cathodic peak maxima. For electrolyte concentrations between 0.0 and 0.12 M ($(TBA)PF_6$) the $E_{1/2}$ value was found to be virtually independent of added electrolyte ($E_{1/2}$ = 0.663 ± 0.006 V vs ferrocene as an internal standard).

## Discussion

**Structural Considerations.** The very close agreement between the X-ray structures of **I** and **II** (at least those parts of the structure of **II** which are not disordered) and the structures obtained by molecular mechanics calculations give us considerable confidence that, first, the modeled results are accurate representations of the structures and, second, the solid-state and solution structures are quite similar. Table 1 lists the Fe−Fe separations obtained from the molecular modeling calculations. Interestingly, while the Fe−Fe distances in **I** and **II** are the same, the increase in Fe−Fe distance upon going from **II** to **III** (1.5 Å) is quite substantial.

(11) (a) O'Dea, J. J.; Osteryoung, J.; Osteryoung, R. A. *Anal. Chem.* **1981**, *53*, 695−701. (b) Junker, P.; Osteryoung, J. North Carolina State University, Personal communication.

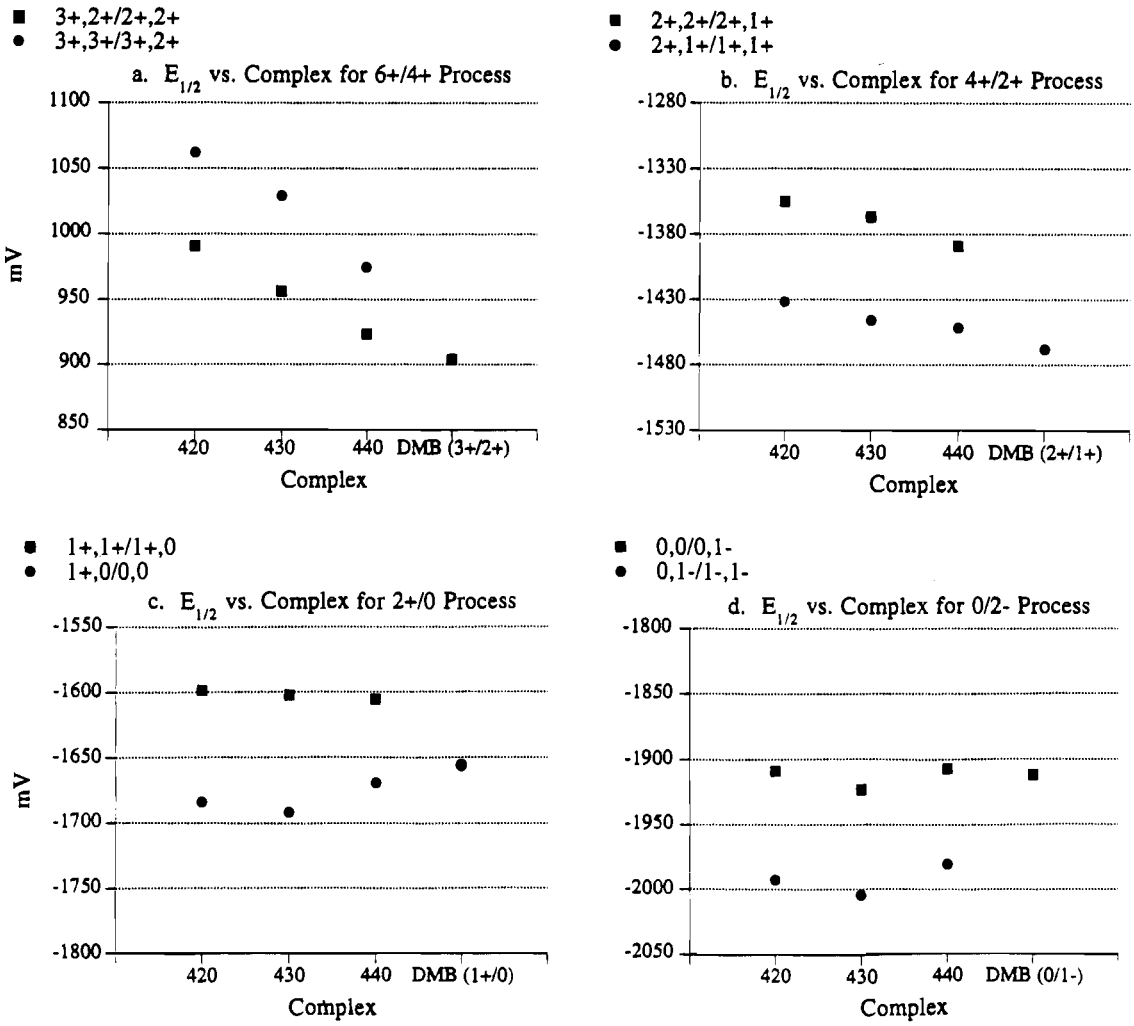


**Figure 4.** $E_{1/2}$ vs complex, as resolved by Osteryoung square wave voltammetry analysis.

**The Nature of the Metal−Metal Interaction.** The saturated nature of the alkyl linkages in **I**−**III** supports the argument that the mode of interaction between the two metal centers in these complexes is largely, if not exclusively, Coulombic. In a separate study the exchange coupling matrix elements have been extracted by a Hush treatment of the very weak intervalence charge transfer transition present in the Fe(II)−Fe(III) mixed-valence forms of **I** and **II**. While the details of that study are presented elsewhere,[12] these data fully support the contention that the site−site interactions expressed in the electrochemical data are virtually exclusively electrostatic in nature (i.e., $H_{12} < 50\ cm^{-1}$). Unfortunately, due to spectral interferences, similar results are not attainable for other mixed valence forms of **I** and **II**; however, INDO calculations for the Fe(I)−Fe(II) form also indicate relatively weak coupling ($H_{12} < 600\ cm^{-1}$). It can be concluded that, in the present context, all of the redox forms of **I**−**III** can be considered to be fully valence localized.

**Choice of a Mononuclear Reference Compound.** Before discussing the details of the electrochemical data, consideration needs to be given to the choice of an appropriate point of reference for comparisons of potentials. Ideally, the exact mononuclear analog of each dinuclear complex would be best for comparison (i.e., $[Fe(\mathbf{420})_3]^{2+}$, $[Fe(\mathbf{430})_3]^{2+}$, and $[Fe(\mathbf{440})_3]^{2+}$). Unfortunately, Fe(II) is modestly labile and the presence of free bipyridines in these complexes makes it impossible to use them as mononuclear analogs. Instead, we have chosen to compare the electrochemical results to $[Fe(DMB)_3]^{2+}$. For complexes **II** and **III** this comparison should be entirely appropriate since the alkyl chain linking the two bipyridines should be electronically equivalent to a methyl substituent. In contrast, since both methyene groups in the alkyl chain of **420** are benzylic, the same type of comparison between $[Fe(DMB)_3]^{2+}$ and $[Fe_2(\mathbf{420})_3]^{4+}$ is more questionable.

In an attempt to evaluate the appropriateness of $[Fe(DMB)_3]^{2+}$ as a mononuclear analog of **I**, we compared the potentials of the 2+/3+ couple in three related substitutionally-inert ruthenium complexes: $[Ru(DMB)_3]^{2+}$, $[Ru(\mathbf{420})_3]^{2+}$, and $[Ru(\mathbf{430})_3]^{2+}$. As anticipated, the $E_{1/2}$ values obtained for the metal-centered oxidation in $[Ru(DMB)_3]^{2+}$ and $[Ru(\mathbf{430})_3]^{2+}$ (and presumably $[Ru(\mathbf{440})_3]^{2+}$, as well) were, within experimental error, identical. Somewhat surprisingly, the oxidation of the $[Ru(\mathbf{420})_3]^{2+}$ complex occurred at a potential ca. 15 mV more positive than for the other two complexes. Assuming that the Fe and Ru complexes behave similarly, differences in potentials between $[Fe(DMB)_3]^n$ and **II** or **III** should reflect only the electrostatic contributions of the second redox site. Comparisons between $[Fe(DMB)_3]^n$ and **I** are more complex due to the presence of slight electronic differences between the ligands in addition to whatever electrostatic effects may be present for this dinuclear complex.

**Electrostatic Contributions−Relative Redox Potentials.** In Figure 4 and Table 2 the $E_{1/2}$ values are presented for the four pairs of redox processes accessible in acetonitrile for **I**−**III** along with the potential for the corresponding process in [Fe-

(12) Derr, D.; Ferrere, S.; Elliott, C. M.; Newton, M. Manuscript in preparation.

$(DMB)_3]^{2+}$. A number of trends can be extracted from this data that can be straightforwardly rationalized based on a purely Coulombic interaction model. Since the data for **I** are complicated by the electronic differences in the ligands (*vide supra*), discussion of this complex will be deferred until the other three have been considered.

The most obvious feature of the data presented in Figure 4 and Table 2 is that the potentials for the various redox processes of **II** and **III** are, in most instances, different from the corresponding process of $[Fe(DMB)_3]^n$. When the dinuclear complexes have a different overall formal charge from that of the mononuclear complex the potentials are shifted relative to those of $[Fe(DMB)_3]^n$. The sign of the shift depends on the sign of the charge on the complex. For example, the dinuclear oxidation (2+,2+/2+,3+) is more difficult than the mononuclear 2+/3+ process (i.e., $E_{1/2}$ is more positive) for both **II** and **III**. In contrast, the two dinuclear reductions: 1+,0/0,0 and 0,0/0,1− occur at very nearly the same potential, respectively, as the mononuclear 1+/0 and 0/1− processes. In each of these latter cases the dinuclear complexes carry the same formal charge as the mononuclear complex. Finally, the 0,1−/1−,1− dinuclear reductions are, again, more difficult (i.e., more negative) than the 0/1− mononuclear process.

The second trend which emerges from a consideration of the potential data in Figure 4 and Table 2 is that the shift in potential relative to that of $[Fe(DMB)_3]^{n/n+1}$ is always larger for **II** than for **III**, and the absolute magnitude of the shift increases with the absolute magnitude of the overall formal charge on the complex. In the most extreme case, the (3+,3+/3+,2+) couple of **II**, the potential is ca. 125 mV more positive than the 3+/2+ couple of $[Fe(DMB)_3]$. Here again the absolute values of the potentials and the trends are in semiquantitative agreement with an electrostatic interaction model discussed below.

The final observation from the data presented in Figure 4 and Table 2 relates to the $\Delta E_{1/2}$ between the members of each adjacent pair of processes in the dinuclear complexes; that is:

$$E_{1/2} = E_{1/2}(n,n/n,n+1) - E_{1/2}(n,n+1/n+1,n+1)$$

For the metal-centered processes, where the charges are largely localized on the iron, $\Delta E_{1/2}$ is ca. 40% bigger for **II** than **III**. For the other processes, which are ligand based, $\Delta E_{1/2}$ is always larger for **II** than **III**, but the relative differences are generally smaller than for the metal-centered process.

With all of the above comparisons in hand, we can now consider the potentials for **I** relative to **II**. In every case the corresponding processes for **I** occur at more positive potentials than for **II**. This result is qualitatively consistent with the observations made for $[Ru(\mathbf{420})_3]^{2+}$ and $[Ru(\mathbf{430})_3]^{2+}$ earlier. The magnitude of the potential difference depends on the specific process considered but is largest for the metal-based oxidations (ca. 34 mV). Since the orbitals involved in each specific redox process are all different, it is not unreasonable that the relative potential shift between these two complexes should change from process to process. The most striking observation, however, comes from comparisons of $\Delta E_{1/2}$. In every case, within ±3 mV, the $\Delta E_{1/2}$ values for each corresponding process in **I** and **II** are the same (cf. Table 2b) which is consistent with the absolute differences in potentials between **I** and **II** being due to electronic differences in the ligands and *not* differences in Coulombic interaction. Thus, by comparing $\Delta E_{1/2}$ the electronic differences between the **420** and **430** ligands are largely factored out. Consequently, $\Delta E_{1/2}$ should be the purest measure of the differences in Coulombic interactions within these dinuclear complexes (*vide infra*).

**The Electrostatic-Interaction Model.** The electrochemical results presented in Figure 4 and Table 2 are all in surprisingly good semiquantitative agreement with a simple electrostatic interaction model employing formal charges for the complexes. When the electrochemistry alters the formal charge on one end of the dinuclear complex the charge of the other end influences the electrochemistry in an entirely predictable way. The magnitude and direction of potential shifts relative to $[Fe(DMB)_3]^n$ are determined by the magnitude and sign of the charge and the distance separating the charges. The shifts are largest for the biggest charges and smallest distance of separation. In the case where the formal charges of the mono- and dinuclear complexes are the same, the potentials are also very nearly the same but not identical (ca. 40 mV in the most extreme case). Even these differences can be straightforwardly rationalized by considering the detailed electronic structures of the complexes. All of the redox processes occurring at negative potentials are primarily ligand based; therefore, treating these reduced complexes as simple point charges located at the metal is obviously a gross oversimplification. The fact that the dinuclear and mononuclear potentials for these formally neutral complexes are in as close agreement as they are is, in fact, more surprising than the existence of small differences.

The two metal-centered processes are the ones for which a simple point-charge model is most nearly appropriate. For that reason we have chosen to take a more quantitative look at these processes in the context of the electrostatic interaction. Several models have been previously used for similar symmetric dinuclear systems. In a singly-bridged dinuclear ruthenium system where the metals were linked by a 4,4′-bipyridyl ligand, Taube and co-workers originally modeled the two ruthenium centers as point charges in a continuum of constant dielectric.[2a] This approach significantly underestimated the electrostatic interaction in the complexes. Because this dielectric continuum model does not account for ionic-strength dependencies of the comproportionation, Taube employed a more involved model in a later publication.[2b,13] Here the ligand-bridged complexes were described by ellipsoids, the parameters of which could be obtained from crystallographic data. The complex was modeled as having a different dielectric constant within the ellipsoid compared to that of the surrounding medium. The electrostatic interaction was approximated by the charges moving away from the foci symmetrically along the major axis. While this approach improved the approximation of the electrostatic contribution, it still underestimated the observed interaction.

In order to determine if the medium between the iron centers for the $[Fe_2(\mathbf{4X0})_3]^{4+}$ complexes could be reasonably approximated by a simple dielectric continuum, we employed microelectrode voltammetry to investigate the electrochemical behavior of these complexes over a range of several orders of magnitude in ionic strength (including *no* added electrolyte). The potential for oxidation of the metal center in **I** was found to be unaffected by changes in the ionic strength of the solution, indicating that there were no significant screening effects due to ions in solution. Most probably, the reason for the differences between our results and those of Taube lie in the nature of the bridge(s) between the two systems. Unlike the singly linked case, the triply bridged nature of our **4X0** complexes excludes solvent and ions from the region between the charges. Thus the charges are largely not screened by ions in solution. Therefore, for our systems, the interaction between the iron centers can be approximated simply by two point charges

(13) (a) Kirkwood, J. G.; Westheimer, F. H. *J. Chem. Phys.* **1938**, *6*, 506. (b) Kirkwood, J. G.; Westheimer, F. H. *J. Chem. Phys.* **1938**, *6*, 513. (c) Ehrenson, S. *J. Am. Chem. Soc.* **1976**, *98*, 7510.

**Table 3.** Calculated $\Delta E_{1/2}$ Values for Bridging Ligands

| | $E_{1/2}$ (mV) | | |
|---|---|---|---|
| solvent | **420** | **430** | **440** |
| $CH_3CN$ | 49 | 49 | 43 |
| pyridine | 154 | 154 | 129 |

separated in a medium of *average* dielectric continuum (i.e., the dielectric of the central region and that of the surrounding solution).

In a dielectric continuum, the electrostatic potential created by a spherical ion $j$, as a function of separation distance r, is approximated by[14]

$$\psi_j(r) = \frac{Q_j}{4\pi\epsilon\epsilon_0 r} \tag{1}$$

where $Q$ is the charge, in coulombs, at each site, $r$ is the separation distance in meters, $\epsilon$ is the dielectric constant of the medium, and $\epsilon_0$ is the vacuum permittivity constant ($8.85419 \times 10^{-12}$ $C^2$ $N^{-1}$ $m^{-2}$). The potential energy of an ion, $i$, at a distance $R_{ij}$ from ion $j$, is equal to the product of the charge on ion $i$ and the potential energy function of ion $j$

$$U_{ij} = Q_i\psi_j(R_{ij}) = \frac{Q_iQ_j}{4\pi\epsilon\epsilon_0 R_{ij}} \tag{2}$$

which is equal to the work required to charge ion $i$ in the presence of ion $j$.

As pointed out above, for the 6+/4+ process this type of model should be reasonably appropriate since most of the charge is localized on the metal centers. First, the electrostatic contribution to the $\Delta E_{1/2}$ for the (3+,3+/2+,3+) and (2+,3+/2+,2+) processes can be calculated by use of this model. The difference in redox potential of the $Fe^{3+/2+}$ couple for an iron center adjacent to a 2+ charge, relative to the potential when it is adjacent to a 3+ charge, can be approximated by use of eq 2. The work required to charge center $i$ (to $Q_i$) in the presence of center $j$ is given by the function

$$W_A = \frac{Q_iQ_j}{4\pi\epsilon\epsilon_0 R_{ij}} \tag{3}$$

If the charge on $j$, $Q_j$, is increased by 1 the work required to charge $i$ to $Q_i$ is

$$W_B = \frac{Q_i(Q_j + 1)}{4\pi\epsilon\epsilon_0 R_{ij}} \tag{4}$$

The difference between eqs 3 and 4 is equal to the work required for the process ($Q_i$,$Q_j$/$Q_i$,$Q_j$ + 1):

$$\Delta W = W_B - W_A = \frac{Q_i}{4\pi\epsilon\epsilon_0 R_{ij}} \tag{5}$$

The difference in work between the individual processes ($Q_i$,$Q_j$/$Q_i$,$Q_j$ + 1) and ($Q_i$,$Q_j$ + 1/$Q_i$ + 1,$Q_j$ + 1) represents the difference in the redox potentials, $\Delta E_{1/2}$, of the coupled processes and is equal to

$$\Delta E_{1/2} = \frac{1}{4\pi\epsilon\epsilon_0 R_{ij}} \tag{6}$$

Table 3 lists calculated $\Delta E_{1/2}$ values obtained from eq 6. The value of $R_{ij}$ employed in the calculation was the Fe−Fe distance obtained from molecular modeling calculations (listed in Table 1). Two sets of $\Delta E_{1/2}$ values are given: one using the dielectric constant of acetonitrile and one using the dielectric constant of pyridine. In every case the calculated $\Delta E_{1/2}$ using the dielectric constant for acetonitrile substantially underestimates the actual experimental values (see Table 2b). As stated above previous attempts at using such a model have likewise tended to underestimate the apparent electrostatic contribution.[2a,4] If eq 6 is used to calculate an effective dielectric constant from experimental $\Delta E_{1/2}$ values (employing Fe−Fe separations in Table 1), the values obtained are 26.7, 26.1, and 30.4, respectively, for **I**, **II**, and **III**. These calculated dielectric constants are between the literature values for acetonitrile (~39) and pyridine (~12). Since the triple linkage in these complexes excludes the solvent and electrolyte from the region between the two charged centers and since that region is filled with pyridine/alkanelike material, it is reasonable that the effective dielectric should lie between these two extremes. Moreover, the calculated dielectric constant for **III** is more acetonitrile-like than are those for **I** and **II**. Again this is consistent with the simple model under consideration. The further apart the charges are the more the electric field penetrates into the acetonitrile; and, thus, the more the effective medium looks like acetonitrile and less like pyridine/alkane.

Additionally, calculations using eq 6 support the argument presented earlier about the values of $\Delta E_{1/2}$ for **I** and **II**. Despite differences in the electronic nature of the ligands, since **I** and **II** have the same metal−metal distances (and, thus, the same value of $R_{ij}$), $\Delta E_{1/2}$ values should be the same, as they are.

Finally, even though the point charge model cannot be rigorously applied to processes involving ligand based reductions there are some qualitative observations that are consistent with an electrostatic model that takes into account the relative locations of charges within the reduced complexes. For a given complex $\Delta E_{1/2}$ increases as the complex becomes more reduced. The smallest $\Delta E_{1/2}$ is observed for the metal based processes and the largest for the 0/2− pair. The closest bipyridine edge-to-edge distance in **I**, for example, is less than half the Fe−Fe distance. If it is assumed that the electrons reducing the bipyridines will be localized so as to minimize electrostatic repulsion, the first pair of electrons should reduce two bipyridines that are as far removed from each other as possible. However, for the next two reductions the second electron of the pair is forced into a position directly across from a previously reduced bipyridine (i.e., the bipyridine on the other end of the alkyl chain is already reduced). Comparisons of the $\Delta E_{1/2}$ values in Table 2b for the three pairs of ligand reductions are roughly consistent with this picture. Particularly for **I** and **II** the $\Delta E_{1/2}$ for the last two pairs of reductions are about the same and both are larger than for the first ligand based reduction. The observation that **III** fits this picture less well may have to do with the fact that it is the most conformationally compliant of all the complexes and therefore may be able to undergo slight structural adjustments in ways that are not possible for **I** and **II**.

**Acknowledgment.** The authors wish to thank Professor Janet G. Osteryoung and her research associates for assistance in obtaining fits to the OSWV data. Helpful discussion with Professor A. K. Rappé and access to his molecular modeling facility is also gratefully acknowledged. Assistance with the X-ray structural work was obtained from Susie M. Miller. This work was supported by the U.S. DOE Office of Basic Energy Science (Grant DE-FG02-92ER14301).

IC950627W

(14) Harned, H. S.; Owen, B. B. *The Physical Chemistry of Electrolytic Solutions*, 2nd ed.; Reinhold: New York, 1950; pp 17−31.